Ligand Engineering of Tetra N-Heterocyclic

Carbenes for Boosting Catalytic Aziridination

Brett A. Smith, Somon Hakimov, David M. Jenkins,* Konstantinos D. Vogiatzis*

Department of Chemistry, University of Tennessee, Knoxville, Tennessee 37996-1600, United

States

Email: jenkins@ion.chem.utk.edu, kvogiatz@utk.edu

Abstract

A comprehensive computational study on the underlying reactivity of iron tetra-NHC complexes for

C₂+N₁ aziridination catalysis is presented. A library of 18 unique iron tetra-NHC complexes was

constructed, and a computational screening was performed on the reaction barriers associated with the

rate-determining step (formation of an open chain radical intermediate). Thermodynamic barriers were

computed along with a variety of steric and electronic properties, including the percentage of buried

volume, orbital energies and ETS-NOCV analysis, which were used to identify key characteristics

related to reactivity. The analysis performed in this study successfully identified key differences in

tetracarbenes, such as linking groups (BMe₂ or CH₂) and the identity of the NHC groups (imidazole,

imidazoline or benzimidazole) in terms of sterics, electronics and thermodynamics. Additionally, we

have proposed two reaction pathways based on electronic structure arguments for the formation of the

1

key open-chain radical intermediate. The first reaction pathway proceeds through a σ -hole channel where the Fe(IV)-imide intermediate evolves into Fe(III)-imidyl radical through electron donation into the antibonding σ^* orbital, while the second involves a Fe(III)-imidyl radical formed through a π -hole channel (donation into π^*). These pathways are consistent with the isoelectronic iron(IV)-oxo species for hydrogen atom abstraction mechanisms and they can be used as descriptors of the rate-determining step of the aziridination reaction.

1. Introduction

Aziridines, the nitrogenous relative to epoxides, are three-membered rings consisting of two carbon atoms and one nitrogen atom. Aziridines are significant in synthetic¹, industrial² and biological applications³, and can be utilized in a variety of different ring-opening and ring expansion reactions to form high-value products⁴. Like other three-membered rings, aziridines experience significant strain energy (\sim 27 kcal/mol⁵) that makes their synthesis inherently dependent on the substrates and their ability to selectively perform an organic ring-closing reaction⁶. Transition metal aziridination catalysts have been developed with the goal of broadening the substrate scope, increasing yields under mild reaction conditions, and improving the enantiomeric purity⁷. The three primary reaction pathways to form an aziridine are shown in Scheme 1 (left). Those include (**A**) the catalytic C_2+N_1 addition reactions, which requires a nitrene source and an alkene substrate, (**B**) the catalytic $C_1N_1+C_1$ reactions, which require a carbene source and an imine substrate, and (**C**) a non-catalytic ring closing approach. The catalytic C_2+N_1 pathway has been studied most extensively due to the relative abundance of alkene substrates and nitrene sources compared to imine substrates and carbene sources.

A catalytic cycle for the C_2+N_1 pathway consists of three primary steps, shown in Scheme 1 (right). Step (1) is the azide addition to the transition metal which leads to formation of metal imide species and release of dinitrogen. Step (2) is the addition of alkene for the formation of an open-chain radical intermediate⁸. The last step (3) involves the formation of aziridine through ring-closure and controls stereoselectivity of the reaction; an immediate ring-closure retains the stereochemistry, while a rotation about the C-N bond scrambles the stereochemistry⁹. Within the C_2+N_1 catalytic cycle, the rate-determining step is dependent on the transition metal catalyst.

$$\begin{array}{c} R_1 \\ R_2 \\ R_4 \\ R_4 \\ \end{array} \begin{array}{c} R_1 \\ \text{(Nitrene)} \end{array} \begin{array}{c} R_1 \\ R_2 \\ \end{array} \begin{array}{c} R_2 \\ R_2 \\ \end{array} \begin{array}{c} R_1 \\ R_2 \\ \end{array} \begin{array}{c} R_2 \\ R_2 \\ \end{array} \begin{array}{c} R_1 \\ R_2 \\ \end{array} \begin{array}{c} R_2 \\ R_2 \\ \end{array} \begin{array}{c} R_1 \\ R_2 \\ \end{array} \begin{array}{c} R_2 \\ R_2 \\ \end{array} \begin{array}{c} R_1 \\ R_2 \\ \end{array} \begin{array}{c} R_2 \\ R_2 \\ \end{array} \begin{array}{c} R_1 \\ R_2 \\ \end{array} \begin{array}{c} R_2 \\ R_2 \\ \end{array} \begin{array}{c} R_1 \\ R_2 \\ \end{array} \begin{array}{c} R_2 \\ R_2 \\ \end{array} \begin{array}{c} R_1 \\ R_2 \\ \end{array} \begin{array}{c} R_2 \\ R_2 \\ \end{array} \begin{array}{c} R_1 \\ R_2 \\ \end{array} \begin{array}{c} R_2 \\ R_2 \\ \end{array} \begin{array}{c} R_1 \\ R_2 \\ \end{array} \begin{array}{c} R_2 \\ R_2 \\ \end{array} \begin{array}{c} R_1 \\ R_2 \\ \end{array} \begin{array}{c} R_2 \\ R_2 \\ \end{array} \begin{array}{c} R_1 \\ R_2 \\ R_2 \\ \end{array} \begin{array}{c} R_2 \\ R_2 \\ \end{array} \begin{array}{c} R_2 \\ R_2 \\ \end{array} \begin{array}{c} R_1 \\ R_2 \\ R_2 \\ \end{array} \begin{array}{c} R_2 \\ R_2 \\ \end{array}$$

Scheme 1. Left: Three potential pathways to form aziridine, (**A**) C_2+N_1 catalytic pathway, (**B**) $C_1N_1+C_1$ catalytic pathway and (**C**) organic ring-closing reaction. Right: Catalytic cycle for the C_2+N_1 pathway: (**1**, blue) addition of azide and release of dinitrogen to form the metal imide, (**2**, green) addition of alkene to form the open-chain radical intermediate, (**2'**-red) undesirable pathway to form metallotetrazene, and (**3**, black) ring-closing to form the aziridine.

In porphyrin-based complexes, the formation of the metal imide species (step (1)) is the rate-determining step^{10, 11}, and the fast alkene addition and ring-closing steps lead to efficient yields and good enantiomeric purity. However, the large thermodynamic barrier of the imide formation can lead to a reduced substrate selection, and the nitrene sources that have been successfully utilized in these cases are limited to iodomine reagants¹²⁻¹⁵, chloramine-T¹⁶, and tosyl azide¹⁷, lowering the atom economy significantly¹⁸. In each of these reagents, a tosyl group is attached to the aziridine nitrogen that must be removed to produce desirable products, which risks a complete loss of product due to the significant strain energy of three-membered rings. An alternative approach to C₂+N₁ aziridination catalysis is by lowering the imide formation barrier, which may lead to the utilization of a broader variety of azides for the synthesis of high-value aziridines without any post-synthetic modification.

N-heterocyclic carbenes (NHCs) are established ligands with great versatility in transition metal catalysis and in many cases, they have replaced phosphines as strong σ-donating ligand of choice¹⁹. The nature of metal-NHC bonding has been a somewhat controversial subject in previous years, as initial claims that NHCs were σ-donors only²⁰ have been revisited in more recent studies. Numerous early studies have provided theoretical evidence of NHC→M π-donation and NHC←M π-backdonation, which together constitute about 18% of the total orbital interaction energy²¹⁻²³. Transition metal tetra N-heterocyclic carbene (tetra-NHCs) complexes on iron offer a thermodynamic profile that follows this approach. With this family of molecular complexes, the rate-determining step becomes the addition of alkene (2), which can permit the use of a broader range of azide sources. However, this introduces the drawback of forming metallotetrazene (2') which is in competition with step (2), since this can trap the catalyst in the metallotetrazene intermediate and can potentially block the catalytic activity.

In 2011, the Jenkins group reported their first generation iron tetra-NHC aziridination catalyst [(Me,EtTCH)Fe]²⁺ and would later report a borate-based analogue, coined the second-generation catalyst [(BMe₂,EtTCH)Fe]²⁺, that is capable of fully aliphatic aziridination^{15, 24-26}. The carbon based tetra-NHC is a strong σ-donor, but the incorporation of borate-groups further increased the σ-donor strength. The increased σ-donation of the tetra-NHCs significantly lowers the activation barrier for the formation of iron(IV)-imide, so much so that the rate-determining step becomes the formation of the open-chain radical intermediate⁹. Lowering the barrier to form the iron(IV)-imide clearly benefits the substrate scope, but there has been little discussion regarding the electronic and steric factors that influence the formation of the open-chain radical intermediate. In general, NHCs have be the subject of numerous studies in attempts to unify the nature of NHC bonding with their remarkable reactivity in transition metal complexes, but the

effects on the electronic and catalytic properties of multiple carbene subunits from a multidentate (tetradentate) NHC complex remain relatively unexplored^{20, 27, 28}.

In this article, we report a comprehensive study that addresses (1) how the bridging atoms within a tetra-NHC affect the electronic and steric properties, (2) how the standard monodentate NHC reactivity descriptors describe reactivity within multidentate NHC complexes, and (3) what reactivity descriptors can be formulated to elucidate means of optimizing the thermodynamic barriers with aziridination with iron tetra-NHC complexes. For that purpose, we have introduced a library of unique iron tetra-NHC complexes to further explore how these effects manifest in the thermodynamic barriers for C_2+N_1 aziridination catalysis. This study extends previous work on the understanding of C_2+N_1 aziridination catalyzed with iron tetra-NHC catalysts in terms of the steric and electronic effects. These calculations lead to the discovery of two competitive reaction channels with distinct electronic structure, and helped us to develop a new descriptor that correlates to the energy activation barrier of the rate-determining step²⁹. Our conclusions support the broadening of the substrate scope without favoring the metallotetrazene intermediate through the incorporation of ligands with increased σ -donating abilities and reduced π -donor abilities to destabilize the metal-azide interaction.

Computational Details

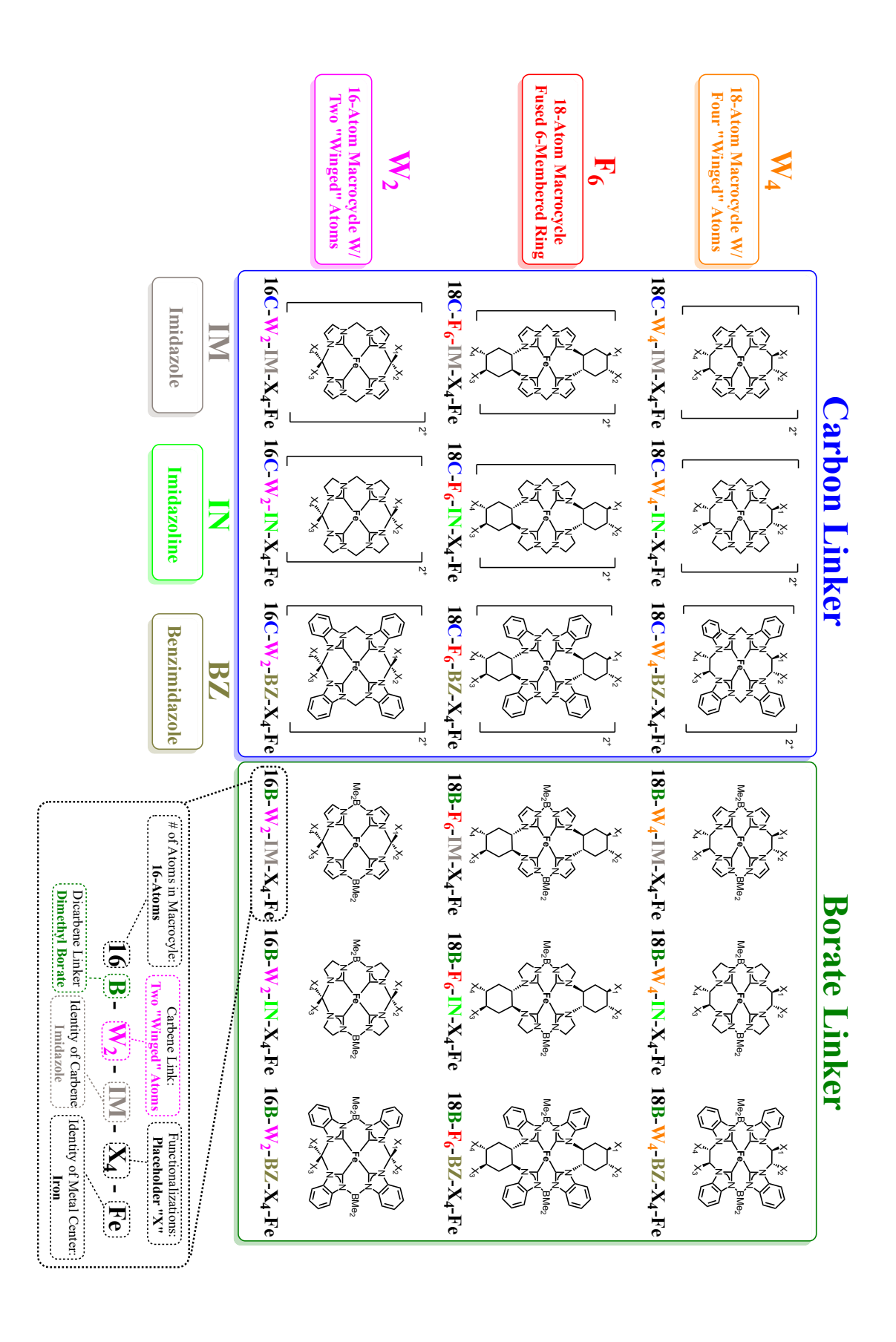
All geometry optimizations and frequency calculations were carried using the ORCA 5.0.2 software package^{30, 31}. First, a benchmark study on the performance of various density functionals was performed (see ESI, Section S1). All results shown herein were obtained with the PBE density functional³², along with Grimme's D3 dispersion correction with Becke-Johnson Damping

(D3(BJ))^{33, 34} and the resolution of identity (RI)³⁵. The def2-SVP basis set was used for all non-iron atoms, while iron employed the def2-TZVP basis set,^{36, 37} with matching auxiliary basis sets. All calculations were carried out with an intermediate spin-state (S = 1), as it is the predicted ground state from DFT, multireference methods and experimental methods^{8, 9, 38, 39}. Additionally the calculation of free volume was performed using SambVca 2.0⁴⁰. All Natural Orbitals for Chemical Valence (NOCV) calculations were carried out in the Multiwfn software package⁴¹. Additional computational details are given in ESI, Section S1.1.

Results and Discussion

Molecular Iron Tetra-NHC Library. Iron tetra-NHC complexes have been employed in aziridination^{25, 42}. Additionally, macrocyclic tetra-NHC complexes have been synthesized using a variety of different transition metals (Cr, Fe, Co, Ni, Rh, Ru, Pd, Pt, and Au)⁴³ as well as group 13 and 14 metals (Sn, In, and Al)⁴⁴. For this project, we have compiled a library of 16 iron tetra-NHCs complexes that utilizes previously reported complexes and new candidate complexes that are potentially viable for aziridination catalysis (Figure 1). The library is organized into two subsets of tetra-NHCs. Tetra-NHCs with a carbon linker between the dicarbenes are shown on the left (blue frame), while those that have a dimethyl borate linker are on the right (green frame). The annotated and magnified expanded name tag (bottom right of Figure 1) further explains the organization and naming convention used for this molecular library. The naming convention is split into five fields separated by a dash "-". The first field (e.g. 16B) is used in identifying the number of atoms in the macrocycle (16-atoms) and what atom connects the dicarbenes (dimethyl borate in this example). The second field "W₂" identifies the connectivity between two carbenes units, the "W" denotes a "winged" complex and its subscript denotes the number of atoms that

have wings. For example, **W**₄ would denote a complex that has four winged atoms in total, whereas **W**₂ would denote a complex that has only two winged atoms. Alternatively, **F**₆ denotes when two carbenes are fused to one another by a six-membered ring. The third field identifies the type of NHC, with **IM**, **IN**, and **BZ** referring to imidazole, imidazoline, and benzimidazole, respectively. The fourth field is used in identifying the identity of the functional groups that are connected to the carbene linker, and the last field is used for the identifying the metal center. Various ligands within this library have been previously synthesized, **18C-W₄-IM-H₄-Fe**¹⁵, **18B-W₄-IM-H₄-Fe**²⁴, **18B-F₆-IM-H₄-Fe**⁴⁵, **16C-W₂-IM-H₄-Fe**⁴⁶, and **16B-W₂-IM-H₄²⁵**. The **16C-W₂-BZ-H₄** complex has been synthesized, but only with a platinum or nickel metal center (**16C-W₂-BZ-H₄-Pt** and **16C-W₂-BZ-H₄-Ni**, respectively)⁴⁷. To date, the only complexes within this library that have been examined computationally are the **18C-W₄-IM-H₄-Fe** and **18B-W₄-IM-H₄-Fe** complexes⁹.



of the dicarbene subunits (dimethyl borate or methyl groups), the overall macrocyclic ring size (16- or 18-atom macrocycles), the linking of the carbene subunits (W_x for x number of atoms that are winged or F_6 for a fused Figure 1. The iron tetra-NHC library introduced in this study. The library organized based on the linking group

Catalytic Reaction Profile of the Aziridination Reaction. The C_2+N_1 catalytic aziridination mechanism has been explored extensively in previous studies^{9, 11, 48}, and there is a consensus for a three-step mechanism, especially for iron-NHC complexes. Those are the addition of azide and subsequent release of dinitrogen to form the iron(IV)-imide intermediate, the addition of alkene leading to the formation of an open-chain radical intermediate, ring-closure to form the final aziridine product. Here, we have recomputed the reaction profile for the 18C-F₆-IM-H₄-Fe, where p-tolyl azide and 1-decene are used as the nitrene source and alkene substrate respectively (see Figure 2). Intermediate 1 corresponds to the α -bound iron(II) azide complex. The first transition state TS₁ leads to the formation of iron(IV)-imide intermediate 2. The second transition state TS₂ results to the iron(III) open-chain radical intermediate 3, while the ring-closing transition state TS₃ leads to the formation of the aziridine.

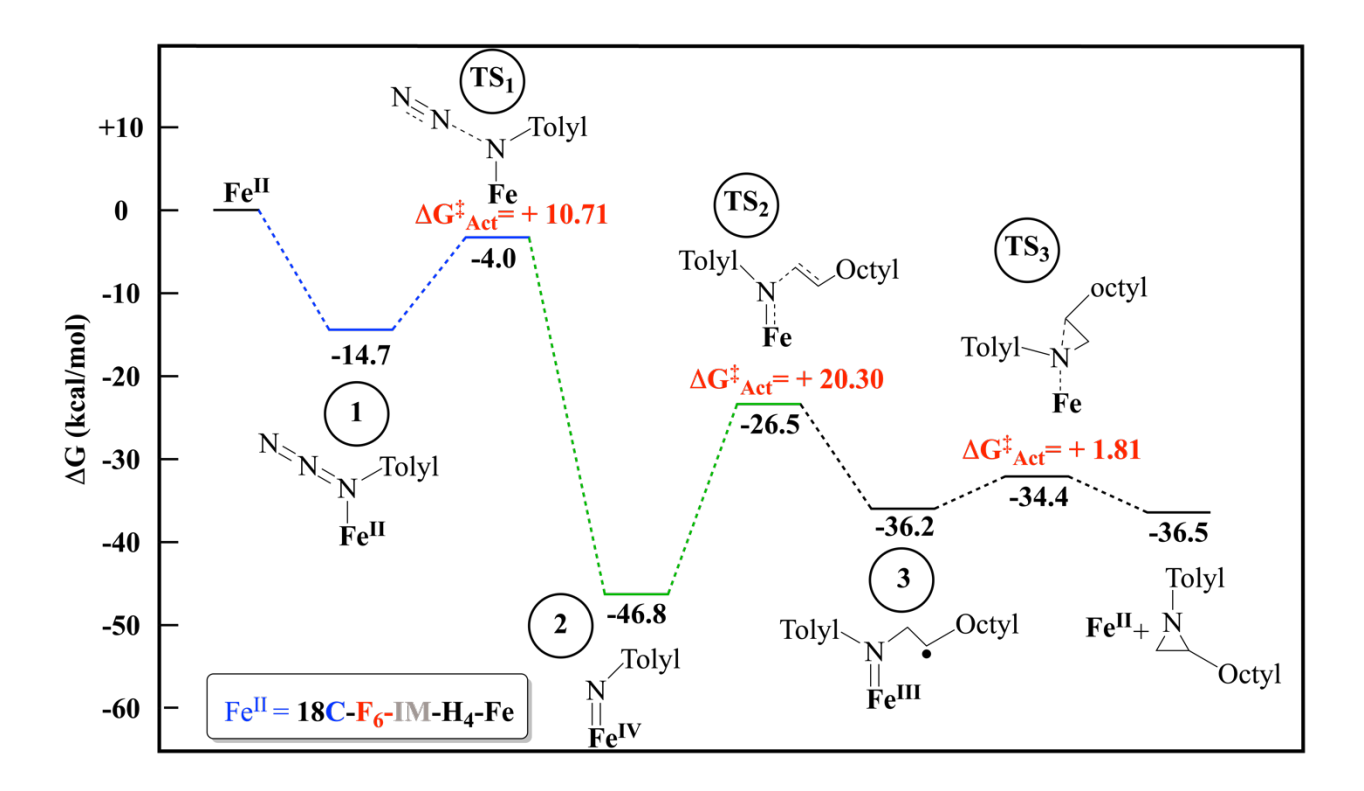


Figure 2. C₂+N₁ mechanism catalyzed by the **18C-F₆-IM-H₄-Fe** complex with para-tolyl azide and 1-decene substrates, as calculated at the PBE-D3(BJ)/def2-SVP/def2-TZVP(Fe) level of theory. Values in black correspond to Gibbs' free energies (in kcal/mol) of an

intermediate/transition state relative to the bare complex and red values correspond to the activation barrier of the corresponding transition states.

The overall efficiency of a potential catalyst should be reflected in the activation energy required to form the open-chain radical intermediate 3 from the iron(IV)-imide intermediate 2, which is the overall rate-determining step of the reaction. For this reason, the primary screening performed for this study consisted the optimization of intermediate 2 and TS₂ for the computation of activation barriers for all complexes in the iron tetra-NHC library which are presented in the bar plots of Figure 3. The dashed horizontal line represents an upper-bound of 25 kcal/mol which corresponds to the previously reported reaction barrier on the aziridination reaction catalyzed by Fe-tetracarbenes⁹ and it is considered here as our reference. The bar plots have been organized based on the dicarbene linker (either carbon or dimethyl borate) and grouped based on the tetracarbene backbone. Tetraimidizoline (IN) are displayed in red bars, tetraimidazole (IM) are displayed in blue, and tetrabenzimidazole (BZ) are displayed in green. As the activation barriers become greater than 25 kcal/mol, the uncatalyzed background reaction (in this case para-tolyl azide reacting with 1-decene to form an aziridine) becomes more favorable than the catalyzed reaction. When this occurs, any benefits offered through catalysis, such as increased yields and selectivity, are significantly diminished.

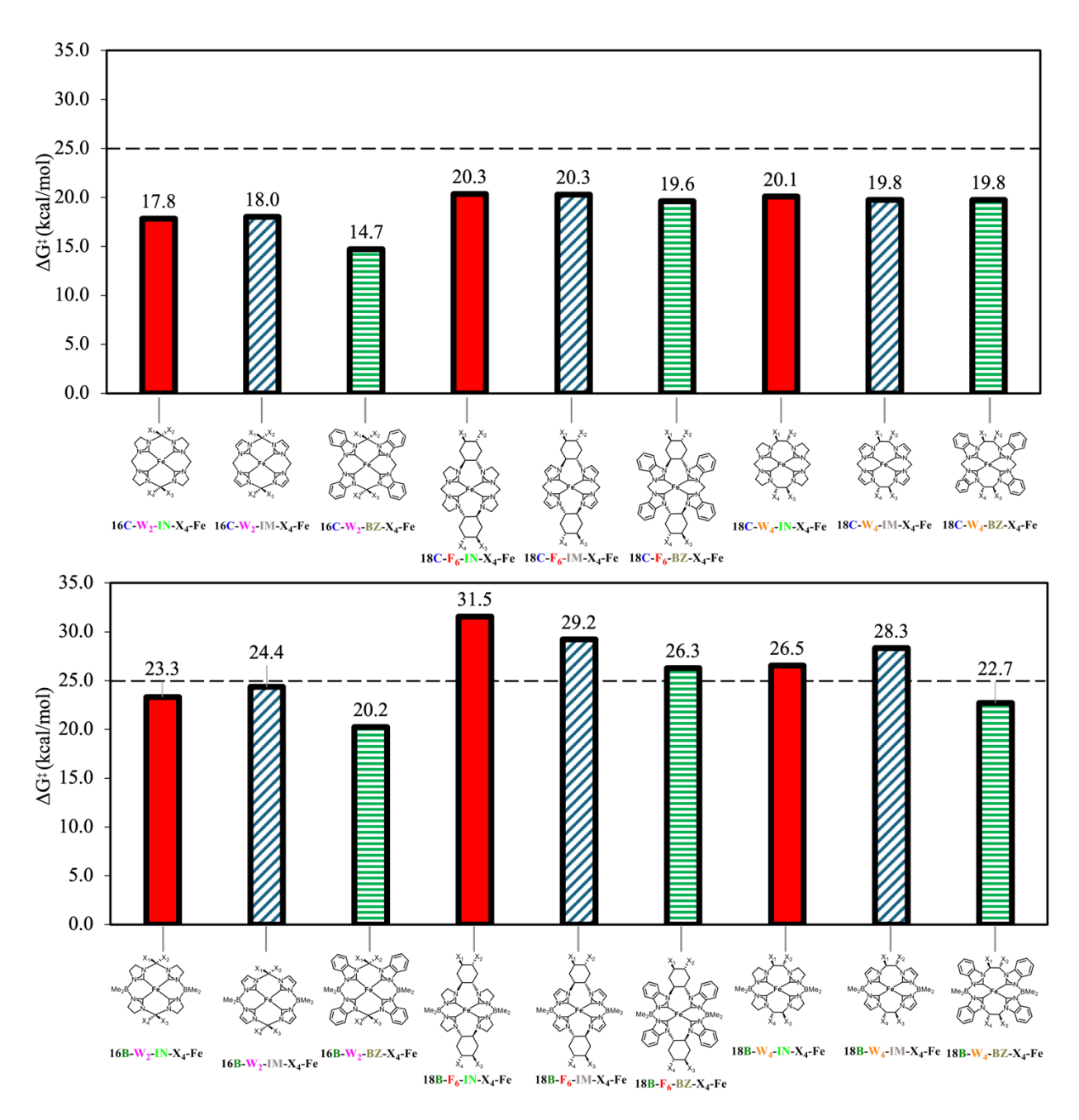


Figure 3. *In-silico* screening of the TS₂ reaction barrier for the iron tetra-NHC library. The top plot corresponds to dicarbene subunits linked through methyl groups, the bottom plot corresponds to dicarbene subunits linked through dimethyl borate groups. The bar plots are further organized based on the macrocycle size, carbene linking groups and carbene subunits. Red bars correspond to imidazoline carbene subunits, blue bars correspond to imidazole carbene subunits and green bars correspond to benzimidazole carbene subunits. All values are in kcal/mol and calculated at the PBE-D3(BJ)/def2-SVP/def2-TZVP(Fe) level of theory.

Steric Effects. The tetra N-heterocylic carbenes chemical space contains a number of different complexes with varying sizes, functional groups and steric bulk effects. For example, 16-atom tetra-NHCs have less steric bulk than the 18-atom tetra-NHC variants. Here, we explore their steric effects and we attempt to correlate those to the reaction barrier of the rate-determining step. There are different methods to describe such steric effects, but in the case of a tetra-dentate ligand, the steric bulk is best described through the use of free and buried volume descriptors. A scatter plot of the free volume as a function of the activation barrier is shown for each family of complexes in Figure 4 (for more information, see Computational Details section and ESI, Section S2). Carbon linked complexes consistently exhibit greater buried volumes and lower activation energies than the dimethyl borate linked complexes. The dimethyl borate groups further distort the planarity of the macrocycle, introducing additional steric hinderance. The average buried volume for the dimethyl borate complexes is 51.6% with an average ΔG^{\ddagger} of 25.8 kcal/mol, and that for the carbon complexes is 44.1% with an average ΔG^{\ddagger} of 19.1 kcal/mol. The buried volume ($V_{\rm bur}$) of the complexes exhibits mostly identical trends across the carbene subunits, 16C-W₂ < 18C-W₂ < 16B- $W_2 \le 18C - F_6 \le 18B - W_4 \le 18B - F_6$, with the last two exchanging for the benzimidazole complexes. It is also important to highlight the trends across different carbene subunits. The tetraimidazole complexes experience the least steric hinderance, with an average $V_{\rm bur}$ of 46% and an average ΔG^{\ddagger} of 23.4 kcal/mol respectively, followed by the tetraimidazoline complexes with an average $V_{\rm bur}$ and ΔG^{\ddagger} of 47.3% and 23.5 kcal/mol and lastly the benzimidazole complexes with an average $V_{\rm bur}$ of 50.4% and an average ΔG^{\ddagger} of 20.6 kcal/mol. These observations highlight that the macrocycle size (16 or 18 atom macrocycle), carbene linking group (CH₂, CH₂CH₂ or C₆H₁₀), and the dicarbene linking group (BMe₂ or CH₂) contribute to the steric effects, and conversely the identity of the carbene subunits (imidazole, imidazoline or benzimidazole) contribute to the electronic

effects far more than the sterics. Additionally, the 18-atom carbon fused macrocycles (18C-F₆) have significant steric bulk (average $V_{\rm bur} = 49.9\%$, average $\Delta G^{\ddagger} = 21.1$ kcal/mol) that does not further affect the reactivity.

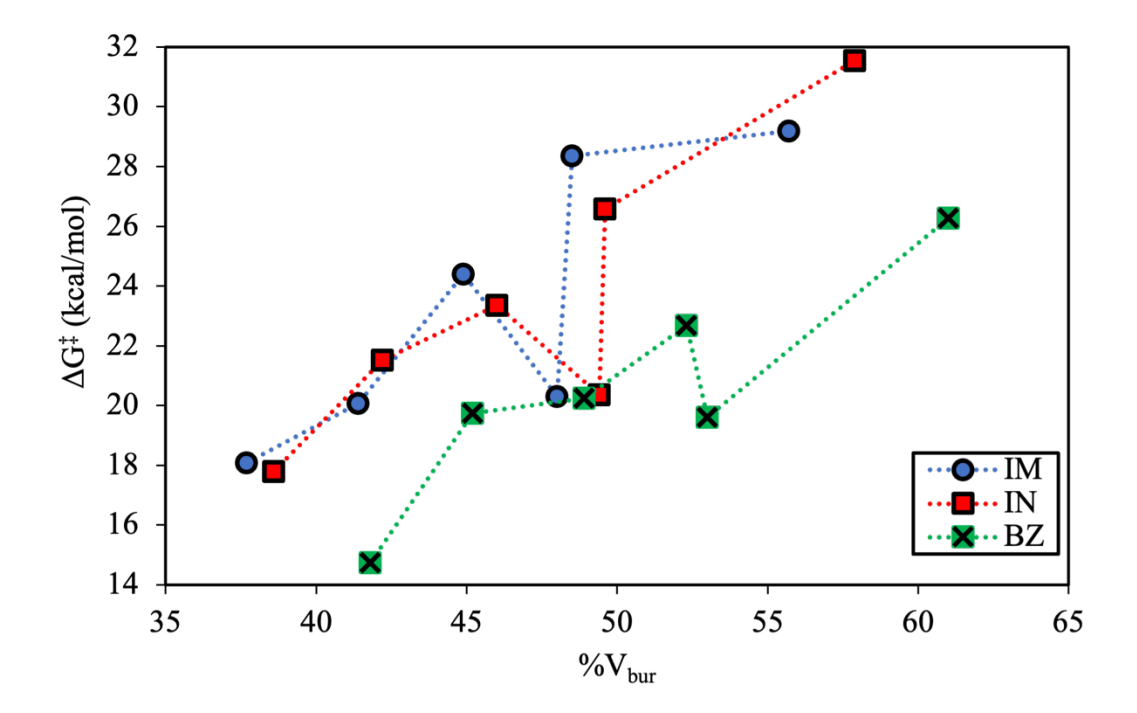


Figure 4. Percent of buried volume (% V_{bur}) of the bare complexes correlated to the alkene addition activation barrier (ΔG^{\ddagger}). Imidazole, imidazoline, and benzimidazole subunits are shown in blue, red, and green, respectively.

NHC-Fe Bonding. Tolman proposed an electronic descriptor for ligand donor abilities in phosphines⁴⁹, based on the work of Strohmeier and Müller⁵⁰. This parameter is based on the C-O stretching frequency of Ni(CO)₃L (where L is the test ligand), and is used in defining the electron donation of a ligand. This parameter has since been adopted in carbene chemistry and provides a valuable ligand descriptor as it can be experimentally measured and theoretically predicted with great accuracy⁵¹. Inspired by the Tolman Electronic Parameter (TEP) descriptor, we have

developed a pseudo-TEP since the use of Ni(CO)3 as a model complex is not entirely viable for the complexes in this study, and thus have utilized the vibrational frequency of a single CO molecule in an axial position to be representative of the ligands donation behavior. The donor strength and nature of donation in the NHC subunits of the molecular complexes of Figure 1 affects the electronic structure of the catalytically active iron center (more detailed information are provided in ESI, Section S2). Thus, it can provide a useful descriptor that characterizes each macrocycle and contributes to the deeper understanding of their reactivity. By extending Tolman's suggestion, we have performed an ETS-NOCV analysis on the three NHC subunits (IM, IN, and **BZ**) to properly characterize the nature of donation within each NHC. For that purpose, we have utilized a model donor-acceptor adduct between each NHC with borane (BH₃). Figure 5 shows the pseudo-TEP value and the results of ETS-NOCV analysis. The results of ETS-NOCV analysis partitions the orbital interaction energy ($\Delta E_{\rm orb}$) into σ - and π -donation and backdonation (where the NHC is the donor and the borane unit is the acceptor). These results nicely show the primary σ-donation of the NHCs ligands (80% of the total electron donation) and align with the conclusions from the pseudo-TEP values, i.e. the strongest σ -donor is imidazoline and the weakest σ -donor is benzimidazole. The remaining 20% of the orbital interaction energy is primarily π -backdonation (or π -accepting of the NHC from BH₃). The order of π -accepting ability follows the order benzimidazole > imidazoline ~ imidazole. In addition to quantitative results, ETS-NOCV analysis provides a qualitative picture of the orbital interaction via the total orbital deformation density, which are shown for these three molecular systems to the right of Figure 5, (electrons flow from blue densities to red densities).

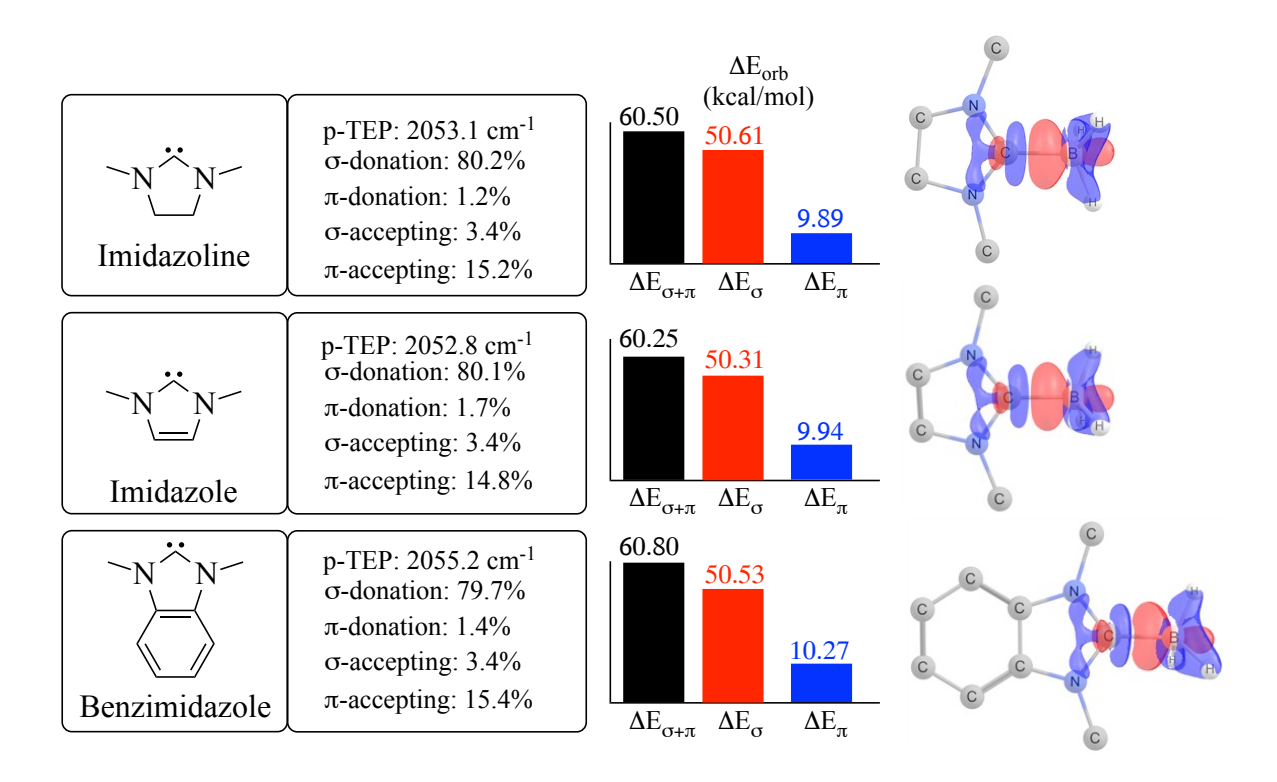


Figure 5. Characterization of the electron donation properties of the imidazoline (top), imidazole (middle) and benzimidazole (bottom) NHCs. The σ - and π -donation and -backdonation from ETS-NOCV analysis is given on the left side, where a BH₃ unit was used as an acceptor fragment. The tabulated results show the pseudo-TEP (p-TEP) values, the percentage of the orbital interaction energy deriving from σ - and π - donation and backdonation. The bar plots depict the ΔE_{orb} values in kcal/mol, black corresponding to the total, red corresponding to σ -donation/backdonation and blue corresponding to π -donation/backdonation. The orbital deformation density is depicted to the far right for each NHC, where blue and red densities represent electron donation (charge depletion) and electron accepting (charge build-up), respectively.

The above analysis provides a description of the donation behavior of monodentate NHCs but despite the rich literature surrounding the nature of NHC-metal bonding^{19, 20, 28, 52}, there have been few studies performed in applying many of the theoretical insights and innovations from mono- and bidentate NHCs onto the tetradentate NHC frameworks.

To further understand the ligands' electronic effects on the rate-determining step of the aziridination reaction, approximate pseudo-TEP values were calculated by placing a CO molecule

on each of the 18 tetra-NHC complexes in axial position. After relaxing the molecular geometries with DFT, the carbon-oxygen vibrational frequency was calculated. The vibrational mode of carbonyl is considered a localized mode with very little coupling to other vibrational modes, and it is only affected by the strength of backdonation from the metal to carbonyl²⁸. The computed vibrational modes v_{CO} for the 16 complexes are shown in Figure 6 as a function of the activation energy ΔG^{\ddagger} of the rate-determining alkene addition reaction step. The pseudo-TEP values show a decrease in $\nu(CO)$ with the decreasing of the π -system, so the order of σ -donor strength becomes imidazoline > imidazole > benzimidazole. The general trend among the varying carbene subunits shows that weaker donors (i.e. better acceptors) require less energy for this rate-determining step. The borate-based complexes are the strongest donors and feature higher activation barriers than their carbon-based counterparts. Additionally, the larger 18-atom fused cyclohexane (18B-F₆) tetra-NHCs are the strongest donors, and also feature the largest activation barriers within their respective groupings. Benzimidazole based complexes are generally the weakest donors and best acceptors, due to their extended π -systems. These findings lead to the following key conclusions: (1) weaker donors stabilize the alkene addition transition state, ultimately lowering the activation barrier, (2) the dimethyl borate groups increase σ -donation and decrease the π -accepting, and (3) larger macrocycles increase the donation abilities.

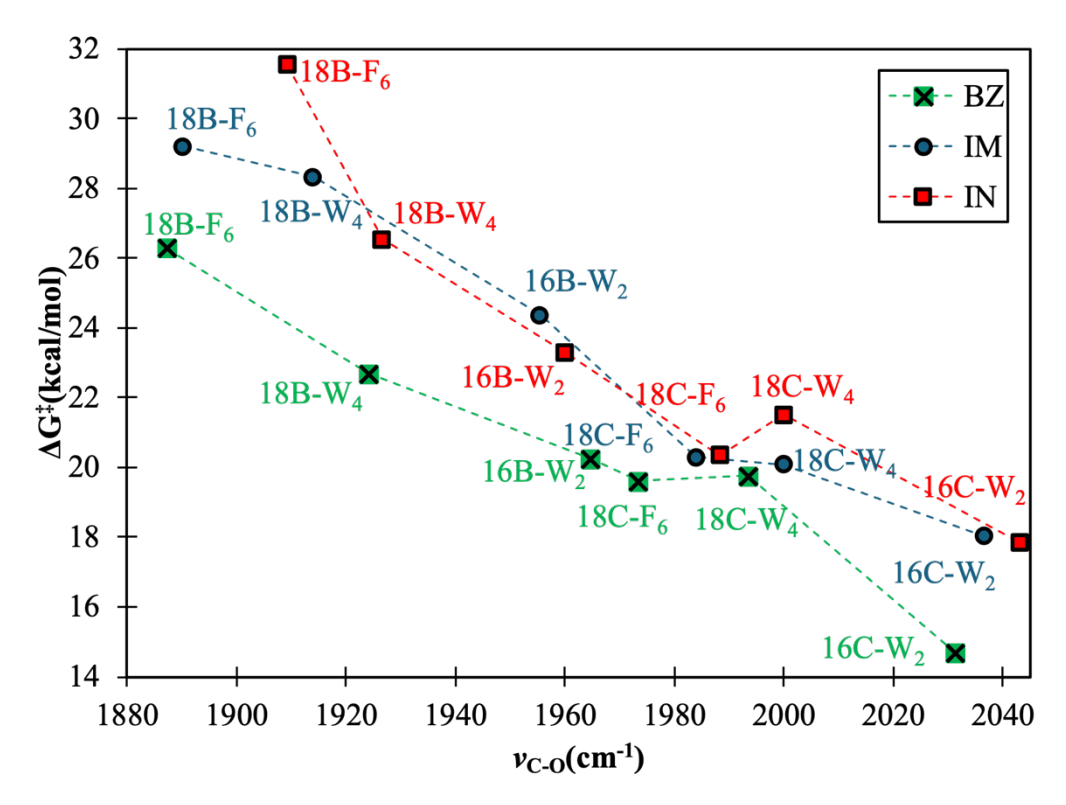


Figure 6. Computed carbonyl vibrational mode for carbonyl bound iron tetra-NHC complexes compared to the activation energy (ΔG^{\ddagger}) for the rate-determing alkene addition (**TS**₂). Imidazole, imidazoline, and benzimidazole subunits are shown in blue, red, and green, respectively.

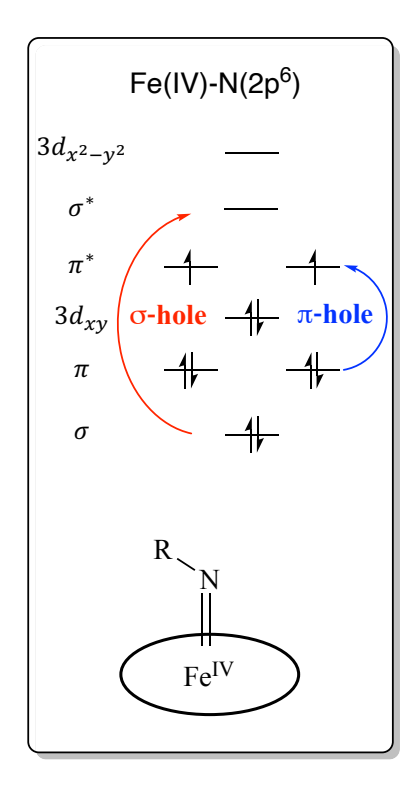
Furthermore, there is a correlation between the pseudo-TEP values and the activation energy, because these two properties are derived from tetra-NHCs bound to different substrates (CO and p-tolyl azide). The pseudo-TEP values express a net effect of donation, as there is no direct methodology on the decoupling of the σ - and π -donation effect on vibrational modes, but nevertheless, the net effects are correlated to this rate-determining activation barrier.

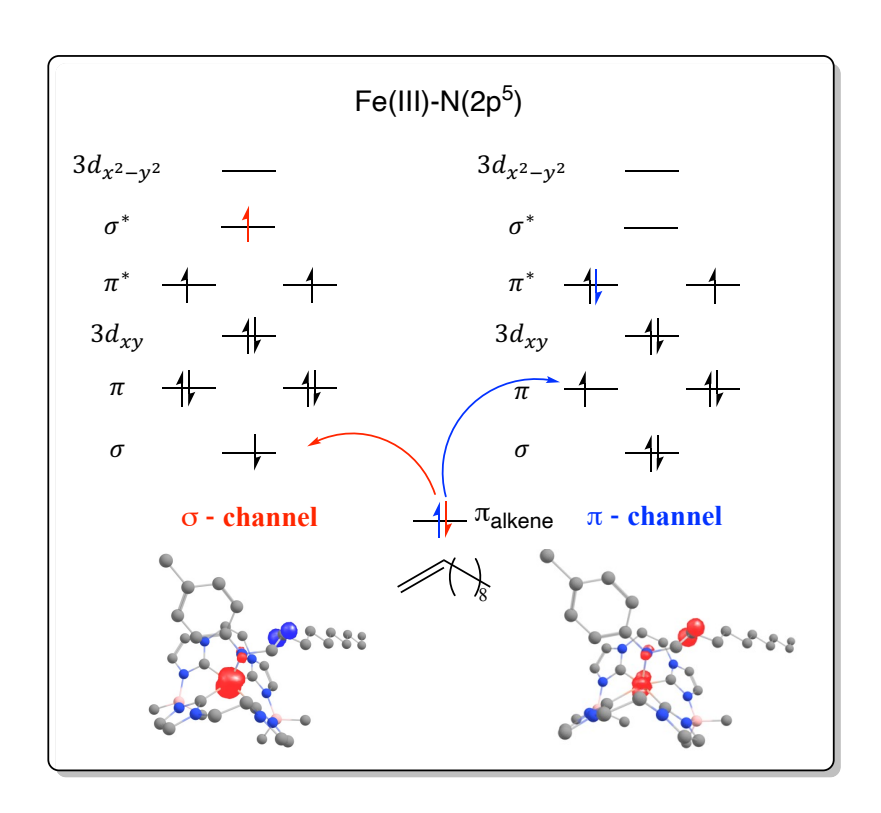
Reaction Mechanisms from Electronic Structure. The versatility of different chemical reactions accelerated by the high-valent iron(IV)-oxo intermediate has been linked to two distinct reaction

channels termed as σ - and π -channels or pathways⁵³. These two channels differ on the character of the radical Fe(III)-O(2p⁵) (or Fe(III)-oxyl) that the Fe(IV)-oxo intermediate evolves during catalytic reactions. In the σ -channel, the unpaired electron of the oxyl radical is found in the $2p_z$ atomic orbital, which participates in the formation of the σ bonding molecular orbital of the Fe(IV)-oxo intermediate. Similarly, the unpaired electron in the π -channel is found in the $2p_{x/y}$ atomic orbital of the oxyl atom. Srnec and coworkers performed an in depth theoretical analysis coupled with magnetic circular dichroism (MCD) spectroscopy to elucidate the underlying effects on σ -reactivity and π -self decay in iron(IV)-oxo complexes⁵⁴⁻⁵⁶. Pandey et al. have used similar electronic structure considerations for the computational examination of the self-amination and self-decay of the [Fe^{II}(6-Ph-TPA)]²⁺ complex (TPA = tris(2-pyridylmethyl)-amine) through a Feimide intermediate⁵⁷. Their analysis was based on previous valence-bond studies on the involvement of the σ^* and π^* orbitals of Fe-imide intermediates on C-H/C=C activation and on reactions with sulfides^{58,59}. These studies showed that σ - and π -channel reactivities can be modulated based on the primary coordination sphere.

We hypothesized that there could be similar effect in iron tetra-NHC aziridination catalysis which leads to two distinct reaction channels. A schematic molecular orbital diagram representation of the σ - and π -channels is shown in Scheme 2. Similarly to the Fe(IV)-oxo chemistry, we found two different channels during the evolution of a Fe(III)-N(2p⁵) configuration from the Fe(IV)-N(2p⁶) intermediate. In the first case, an alpha electron is transferred from the σ to the σ * molecular (σ -channel), which consecutively creates a σ -hole in the electronic structure of the N atom, since the bonding σ orbital has a predominant N character. This intermolecular electron transfer demonstrates the reduction of Fe(IV) to Fe(III) and the formation of a radical on the N atom, similar to the oxyl formation in the Fe(IV)-oxo chemistry. In the second case, this

process occurs between the π/π^* molecular orbitals which creates a π -hole. Since the π^* orbital is already half occupied by an alpha electron, the π -channel involves the transfer of a beta spin electron. The formation of the N-C bond occurs with a one electron donation from the π orbital of the alkene (π_{alkene}), which can have either alpha or beta spin. In the σ -channel, an alpha spin electron fills the σ -hole, leaving a beta spin electron in the π_{alkene} orbital, which is antiferromagnetically coupled to the iron(III) spin center. In the π - channel, a beta electron from the π_{alkene} orbital fills the π -hole, and the alkene is ferromagnetically coupled to the iron(III) spin center. In both cases, the triplet spin state is preserved, but the σ-mechanism produces a brokensymmetry state with four unpaired electrons (three alpha on iron and one beta on the carbon chain). We would like also to note that the electronic structure consideration of the σ/π -holes of Scheme 2 are identical to the description of an electron transferred directly from the substrate to the σ^* or π^* orbital. Overall, the σ -mechanism is expected to be favored for the iron tetra-NHC complexes over the π -mechanism. To verify this, we have computed the energy difference between the two spin states for the 18B-W4-IM-H4-Fe complex, and we found that the spin state that leads to the σ-mechanism is more stable by -9.1 kcal/mol.





Scheme 2. Left: qualitative molecular orbital diagram of the Fe(IV)-N(2p⁶) intermediate together with the formation of two possible electron holes upon reduction of Fe and its evolution to Fe(III)-N(2p⁵). Right: the electronic structure of the Fe-N unit upon N-C bond formation for both σ - and π -channels. The computed spin densities for the two channels are shown at the bottom (antiferromagnetic coupling for the σ -channel).

The HOMO-LUMO gap of the iron(IV)-imide species, which corresponds to the difference in energy of the occupied π^* and unoccupied σ^* , is a useful descriptor for the σ -mechanism reactivity, as it is essentially the energy difference between the orbitals of interest in the reaction. Additionally, the difference in energy of the alpha LUMO (σ^*) and the beta LUMO+1 (π^*) is also a useful reactivity descriptor (Figure 7). The orbital energy difference between these two indicates the relative accessibility of the σ -mechanism, which correlates to the activation barriers. These orbital energy differences are displayed as a function of the activation barrier in Figure 7, additionally the HOMO-LUMO gap of α -spin orbitals, HOMO-LUMO gap of β -spin orbitals, the

 $HOMO(\alpha)$ -LUMO(β) gaps and the absolute energy of the σ^* and π^* orbitals have been displayed as a function of the activation barrier in the ESI, Section S3, Figures S-6 – S-9.

We have also attempted to correlate the exact σ^* and π^* orbital energies with the computed activation barriers. The absolute orbital energies depend greatly on the dicarbene linking group (either dimethyl borate or CH₂). The dimethyl borate complexes have a neutral charge whereas the carbon-based complexes have a 2+ charge, leading to a significant difference in absolute orbital energy (5.6 eV on average). In contrast, the σ^* - π^* metric provides an energy that is internally relative to the complex, and thus is more suitable for comparing complexes with different overall charge. There is a clear difference between dicarbenes linked through borate and carbon, the carbon linked complexes have considerably lower orbital energy differences and lower activation energies. The inclusion of dimethyl borate groups leads to a more electron deficient iron(IV)imide, with similar σ -donation abilities, but is hindered by the lack of π -donation/backdonation abilities that are present in the carbon linked complex. Additionally, most of the lowest activation barriers are in complexes with benzimidazole NHC subunits, suggesting that increased π -accepting ability stabilizes the open-chain radical intermediate. The overall findings for the screening of TS₂ show that the carbon linked complexes experience lower activation barriers than that of the borate linked complexes, which is supported by the buried volume and the orbital energy differences. Additionally, the benzimidazole carbene subunits support the lowest barriers, and the imidazole and imidazoline subunits experience similar activation barriers. Based on the above analysis, we have selected a few representative complexes (16C-W₂-IN-H₄-Fe, 16C-W₂-BZ-H₄-Fe, 18C-F₆-BZ-H₄-Fe, 16B-W₂-IN-H₄-Fe, 16B-W₂-BZ-H₄-Fe, 18B-W₄-BZ-H₄-Fe) for the computation of the complete reaction profile.

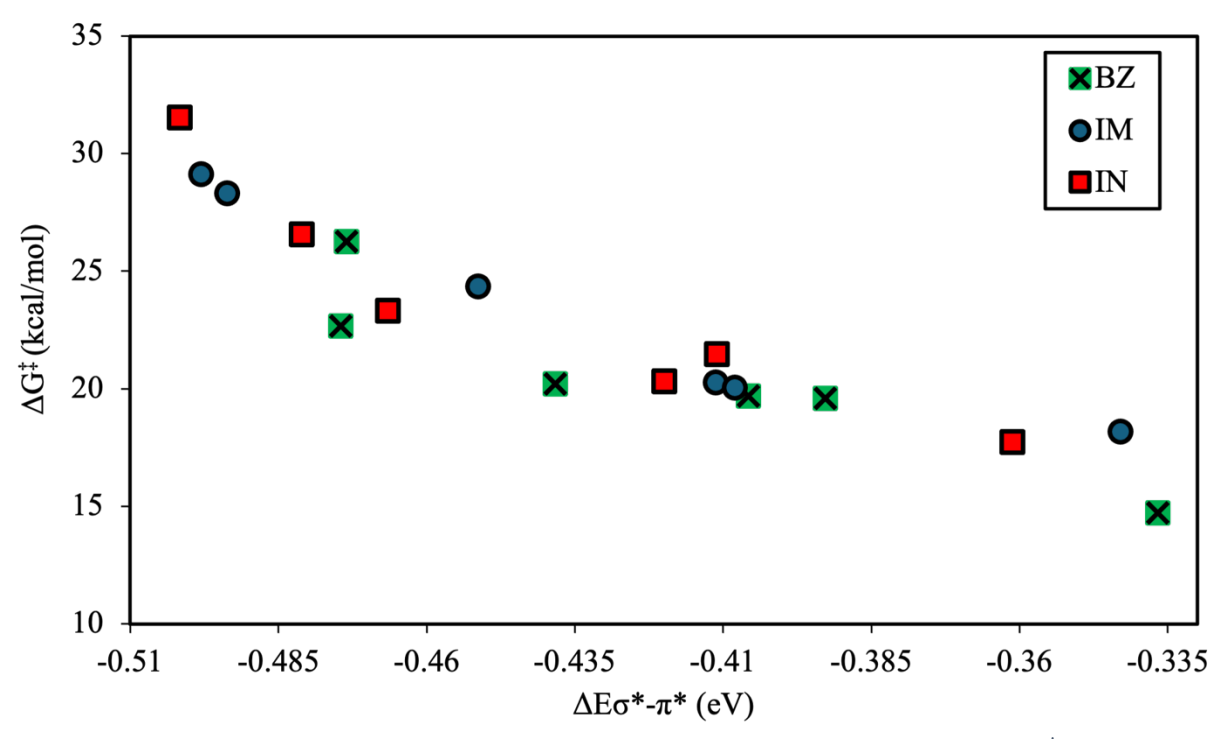


Figure 7. Scatter plots of the HOMO-LUMO (σ^* - π^*) energy gap, in eV, vs ΔG^{\ddagger} , in kcal/mol) for complexes with; imidazoline subunits (top), imidazole subunits (middle) and benzimidazole subunits (bottom).

Extended Screening. The activation energy associated with the formation of the iron(IV)-imide species consists of binding of the azide species (p-tolyl azide) and the release of dinitrogen. The underlying electronic effects associated with this barrier are more well known, the σ -donation abilities directly influenced the relative energy needed to overcome this barrier. The inclusion of dimethyl borate linking groups have been theorized to be stronger σ -donors that those with the carbon linking groups, this finding is consistent with the fact that $18B-W_4-IM-H_4-Fe$ is the only aziridination catalyst that can support a fully aliphatic aziridine (alkyl azides). The results of this secondary screening are shown below in (Figure 8). This secondary screening reaffirmed prior intuition that the dimethyl borate groups support lower activation barriers for the formation of iron(IV)-imide.

To further analyze the underworking of this activation barrier, we have performed extended transition state natural orbitals for chemical valence (ETS-NOCV)⁶⁰. ETS-NOCVs provide three descriptors of chemical (1) chemical valence eigenvalues (ν_k) that correspond to the amount of electron density exchanged in a particular NOCV, (2) the orbital mixing of fragments (ΔE_{ORB}) and, (3) qualitative natural orbitals for chemical valence that describe donor-acceptor interactions. Each descriptor can be further partitioned into σ - and π - forward and back-donation contributions. The chemical valence eigenvalues can be found in below in Table 1. For each complex there are 4 NOCVs (two α and two β) that can be considered significant to bonding (chemical valence eigenvalues above 0.1), of those four the primary σ -donation corresponds to the first α -NOCV. The remaining contributions are series of back-donation from N₂ to the iron and α -bound nitrogen. This NOCV is heavily correlated to the reactivity of the azide bound species to form the iron(IV)-imide, this is shown in Figure 8, where the eigenvalue corresponding to σ -donation from metal to nitrogen is plotted against the activation barrier. The activation barriers of the carbon linked

complexes 18C-W₄-BZ-H₄-Fe, 18C-F₆-BZ-H₄-Fe, and 18C-W₄-IN-H₄-Fe are 11.06, 11.22 and 11.47 kcal/mol, respectively. The activation barriers of the borate linked complexes 16B-W₂-IN-H₄-Fe, 16B-W₂-BZ-H₄-Fe, and 18B-W₄-BZ-H₄-Fe are 4.39, 5.29 and 6.62 kcal/mol, respectively. Thus, we conclude that the ETS-NOCV results support the stronger sigma donation of the borate linked complexes, which further explain the lower iron(IV)-imide formation barriers and larger barriers in the formation of the open-chain radical intermediate.

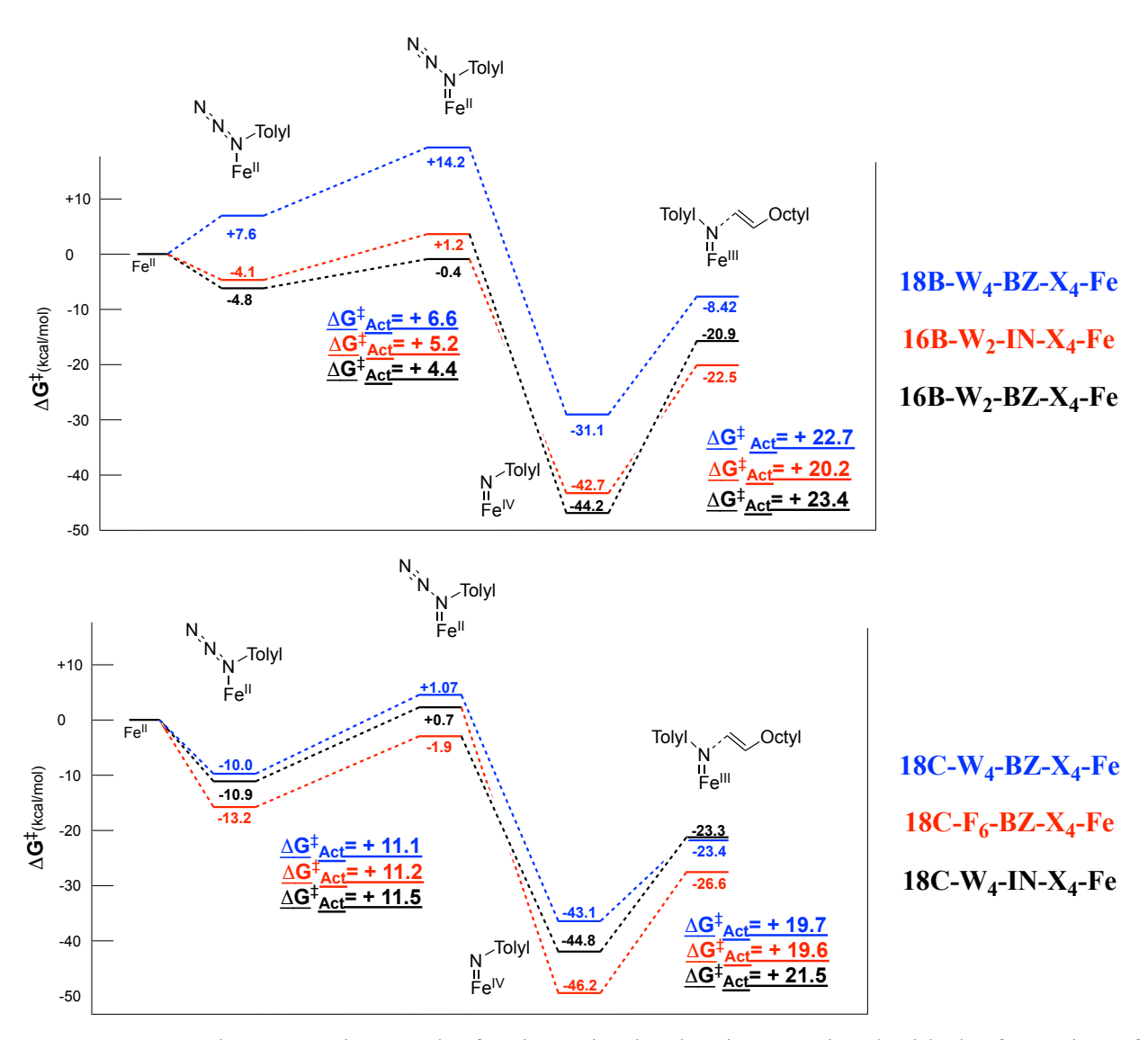


Figure 8. Secondary screening results for the activation barrier associated with the formation of the iron(IV)-imide intermediate (in kcal/mol).

Complex	α1	α2	β1	β2	ΔG^{\ddagger}
16B-W ₂ -IN-H ₄ -Fe	0.283	0.142	0.525	0.264	4.39
$16 \text{B-W}_2\text{-BZ-H}_4\text{-Fe}$	0.285	0.124	0.358	0.169	5.29
$18\text{B-W}_4\text{-BZ-H}_4\text{-Fe}$	0.246	0.112	0.315	0.147	6.62
18C-W ₄ -BZ-H ₄ -Fe	0.222	0.132	0.506	0.238	11.06
18C-F_6 -BZ- H_4 -Fe	0.210	0.134	0.315	0.147	11.22
$18C-W_4-IN-H_4-Fe$	0.214	0.132	0.406	0.234	11.47

Table 1. Tabulated results from ETS-NOCV calculations for each complex in the secondary screening. $\alpha 1$ and $\alpha 2$ correspond to the NOCV eigenvalues (v_k) for the first and second α -NOCVs respectively. $\beta 1$ and $\beta 2$ correspond to the NOCV eigenvalues of the first and second β -NOCVs respectively. All eigenvalues represent fractional values of charge transferred.

Conclusions and Outlook

C₂+N₁ aziridination catalysis with iron tetra-NHC catalysts has made significant growth in recent years. For the purposes of this study, we have compiled a dataset of 18 iron complexes with different variations of tetra-NHC ligands. One of these 18 complexes (**18B-W₄-IM-H₄-Fe**) has been reported to catalyze a fully aliphatic aziridine, while another (**18C-W₄-IM-H₄-Fe**) exhibits some of the highest aziridine yields. Both complexes bare imidazolate units (**IM**) in their ligand structure. Based on our prior knowledge, we believe that the next generation of tetra-NHC C₂+N₁

aziridination catalysts should combine the wide substrate scope of the dimethyl borate-based catalysts and the catalytic efficiency of the carbon-based catalysts.

The reaction barrier of the rate-determining step (formation of the open-chain radical intermediate) was computed for all 18 complexes. Our results showed that, on average, the lowest activation barriers of the NHC subunits were achieved for the benzimidazole complexes. Thus, changing the identity of the NHC groups from imidazole to benzimidazole is a promising molecular engineering strategy that can increase the efficiency of aziridine formation. As a next step, and in order to provide an in-depth understanding on the factors that enhance the catalytic efficiency, we have considered different geometric and electronic descriptors. We then explored how those factors correlate to the computed reaction barriers. We found that the carbon-based complexes exhibit lower activation barriers than those that incorporate stronger σ-donation from dimethyl borate groups.

In addition, a careful analysis of the electronic structure of the key Fe(IV)-imide intermediate revealed two different reaction channels that lead to two different spin configurations. Based on these channels, we proposed a new electronic structure descriptor that correlates to the computed reaction barriers. Finally, after the first screening of the 18 complexes, we have selected six candidate complexes (16C-W2-IN-H4-Fe, 16C-W2-BZ-H4-Fe, 18C-F6-BZ-H4-Fe, 16B-W2-IN-H4-Fe, 16B-W2-BZ-H4-Fe, and 18B-W4-BZ-H4-Fe) to test the first transition state (formation of iron(IV) imide), as this activation barrier is associated with the substrate tolerance. The secondary screening reaffirmed the notion that stronger σ-donation (from dimethyl borate) lowers this activation barrier. We believe that these six molecular complexes are good synthetic targets for the development of the next generation of iron tetra-NHC catalysts for C2+N1 aziridination. Future computational studies from our group will involve correlated methods such as the domain-

based local pair natural orbital coupled-cluster singles-and-doubles with correlated triples method (DLPNO-CCSD(T)) for the further refinement of the calculated reaction barriers, as well as exploration of a larger number of tetracarbene ligands by application of machine learning workflows trained on accurate quantum chemical data.

Acknowledgments:

B.A.S., D.M.J., and K.D.V. are grateful to the NIH (R15GM117494-02) for financial support. This work was partially supported by the National Science Foundation under Grant CHE 2154697. Any opinions, findings, and conclusions expressed in this material are those of the authors and do not necessarily reflect the views of the National Science Foundation. The authors acknowledge the Infrastructure for Scientific Applications and Advanced Computing (ISAAC) of the University of Tennessee for computational resources.

Electronic Supplementary Information

Electronic supplementary information (ESI) available: density functional benchmarking, free volume, steric-mapping, key bond lengths and Tolman electronic parameters, frontier molecular orbital analysis, orbital energies, and orbital energy differences.

Conflicts of Interest

The authors declare no competing financial interest.

References

- (1) Hu, X. E. Nucleophilic ring opening of aziridines. *Tetrahedron* **2004**, *60* (12), 2701-2743. DOI: https://doi.org/10.1016/j.tet.2004.01.042.
- (2) Dremer, O. C.; Ham, G. E. *ETHYLENIMINE AND OTHER AZIRIDINES, CHEMISTRY AND APPLICATIONS*; Academic Press, 1969.
- (3) Andrez, J.-C. Mitomycins syntheses: a recent update. *Beilstein Journal of Organic Chemistry* **2009**, *5*. DOI: 10.3762/bjoc.5.33 (accessed 2023-11-28T18:51:29).
- (4) Sabir, S.; Kumar, G.; Verma, V. P.; Jat, J. L. Aziridine Ring Opening: An Overview of Sustainable Methods. *ChemistrySelect* **2018**, *3* (13), 3702-3711. DOI: https://doi.org/10.1002/slct.201800170 (accessed 2023/11/28).
- (5) Planells, A. R.; Ferao, A. E. Accurate Ring Strain Energy Calculations on Saturated Three-Membered Heterocycles with One Group 13–16 Element. *Inorganic Chemistry* **2020**, *59* (16), 11503-11513. DOI: 10.1021/acs.inorgchem.0c01316.
- (6) Pan, B.; Li, F.; Zhao, Y. Synthesis and applications of methyleneaziridines. *RSC Advances* **2020**, *10* (64), 39304-39322, 10.1039/D0RA07663E. DOI: 10.1039/D0RA07663E.
- (7) Chandrachud, P. P.; Jenkins, D. M. Transition Metal Aziridination Catalysts. In *Encyclopedia of Inorganic and Bioinorganic Chemistry*, 2017; pp 1-11.
- (8) Blatchford, K. M.; Mize, C. J.; Roy, S.; Jenkins, D. M. Toward asymmetric aziridination with an iron complex supported by a D2-symmetric tetra-NHC. *Dalton Transactions* **2022**, *51* (16), 6153-6156, 10.1039/D2DT00772J. DOI: 10.1039/D2DT00772J.
- (9) Isbill, S. B.; Chandrachud, P. P.; Kern, J. L.; Jenkins, D. M.; Roy, S. Elucidation of the Reaction Mechanism of C2 + N1 Aziridination from Tetracarbene Iron Catalysts. *ACS Catalysis* **2019**, *9* (7), 6223-6233. DOI: 10.1021/acscatal.9b01306.
- (10) Lyaskovskyy, V.; Suarez, A. I. O.; Lu, H.; Jiang, H.; Zhang, X. P.; de Bruin, B. Mechanism of Cobalt(II) Porphyrin-Catalyzed C–H Amination with Organic Azides: Radical Nature and H-Atom Abstraction Ability of the Key Cobalt(III)–Nitrene Intermediates. *Journal of the American Chemical Society* **2011**, *133* (31), 12264-12273. DOI: 10.1021/ja204800a.
- (11) Zardi, P.; Pozzoli, A.; Ferretti, F.; Manca, G.; Mealli, C.; Gallo, E. A mechanistic investigation of the ruthenium porphyrin catalysed aziridination of olefins by aryl azides. *Dalton Transactions* **2015**, *44* (22), 10479-10489, 10.1039/C5DT00951K. DOI: 10.1039/C5DT00951K.
- (12) Yudin, A. K. Aziridines and Epoxides in Organic Synthesis; Wiley Online Books 2006.
- (13) Abu-Omar, M. M. High-valent iron and manganese complexes of corrole and porphyrin in atom transfer and dioxygen evolving catalysis. *Dalton Transactions* **2011**, *40* (14), 3435-3444, 10.1039/C0DT01341B. DOI: 10.1039/C0DT01341B.
- (14) Fantauzzi, S.; Caselli, A.; Gallo, E. Nitrene transfer reactions mediated by metallo-porphyrin complexes. *Dalton Transactions* **2009**, (28), 5434-5443, 10.1039/B902929J. DOI: 10.1039/B902929J.
- (15) Cramer, S. A.; Jenkins, D. M. Synthesis of Aziridines from Alkenes and Aryl Azides with a Reusable Macrocyclic Tetracarbene Iron Catalyst. *Journal of the American Chemical Society* **2011**, *133* (48), 19342-19345. DOI: 10.1021/ja2090965.
- (16) Aviv, I.; Gross, Z. Corrole-based applications. *Chemical Communications* **2007**, (20), 1987-1999, 10.1039/B618482K. DOI: 10.1039/B618482K.
- (17) Omura, K.; Murakami, M.; Uchida, T.; Irie, R.; Katsuki, T. Enantioselective Aziridination and Amination Using p-Toluenesulfonyl Azide in the Presence of Ru(salen)(CO) Complex. *Chemistry Letters* **2003**, *32* (4), 354-355. DOI: 10.1246/cl.2003.354 (accessed 2023/11/28).

- (18) Jenkins, D. M. Atom-Economical C2 + N1 Aziridination: Progress towards Catalytic Intermolecular Reactions Using Alkenes and Aryl Azides. *Synlett* **2012**, *23*, 1267 1270.
- (19) Cavallo, L.; Correa, A.; Costabile, C.; Jacobsen, H. Steric and electronic effects in the bonding of N-heterocyclic ligands to transition metals. *Journal of Organometallic Chemistry* **2005**, *690* (24), 5407-5413. DOI: https://doi.org/10.1016/j.jorganchem.2005.07.012.
- (20) Jacobsen, H.; Correa, A.; Poater, A.; Costabile, C.; Cavallo, L. Understanding the M(NHC) (NHC=N-heterocyclic carbene) bond. *Coordination Chemistry Reviews* **2009**, *253* (5), 687-703. DOI: https://doi.org/10.1016/j.ccr.2008.06.006.
- (21) Tonner, R.; Heydenrych, G.; Frenking, G. Bonding Analysis of N-Heterocyclic Carbene Tautomers and Phosphine Ligands in Transition-Metal Complexes: A Theoretical Study. *Chemistry An Asian Journal* **2007**, *2* (12), 1555-1567. DOI: https://doi.org/10.1002/asia.200700235 (accessed 2023/11/28).
- (22) Hu, X.; Castro-Rodriguez, I.; Olsen, K.; Meyer, K. Group 11 Metal Complexes of N-Heterocyclic Carbene Ligands: Nature of the MetalCarbene Bond. *Organometallics* **2004**, *23* (4), 755-764. DOI: 10.1021/om0341855.
- (23) Hu, X.; Meyer, K. New tripodal N-heterocyclic carbene chelators for small molecule activation. *Journal of Organometallic Chemistry* **2005**, *690* (24), 5474-5484. DOI: https://doi.org/10.1016/j.jorganchem.2005.07.119.
- (24) Bass, H. M.; Cramer, S. A.; Price, J. L.; Jenkins, D. M. 18-Atom-Ringed Macrocyclic Tetra-imidazoliums for Preparation of Monomeric Tetra-carbene Complexes. *Organometallics* **2010**, *29* (15), 3235-3238. DOI: 10.1021/om100625g.
- (25) Bass, H. M.; Cramer, S. A.; McCullough, A. S.; Bernstein, K. J.; Murdock, C. R.; Jenkins, D. M. Employing Dianionic Macrocyclic Tetracarbenes To Synthesize Neutral Divalent Metal Complexes. *Organometallics* **2013**, *32* (7), 2160-2167. DOI: 10.1021/om400043z.
- (26) Chandrachud, P. P.; Bass, H. M.; Jenkins, D. M. Synthesis of Fully Aliphatic Aziridines with a Macrocyclic Tetracarbene Iron Catalyst. *Organometallics* **2016**, *35* (11), 1652-1657. DOI: 10.1021/acs.organomet.6b00066.
- (27) Perrin, L.; Clot, E.; Eisenstein, O.; Loch, J.; Crabtree, R. H. Computed Ligand Electronic Parameters from Quantum Chemistry and Their Relation to Tolman Parameters, Lever Parameters, and Hammett Constants. *Inorganic Chemistry* **2001**, *40* (23), 5806-5811. DOI: 10.1021/ic0105258.
- (28) Gusev, D. G. Electronic and Steric Parameters of 76 N-Heterocyclic Carbenes in Ni(CO)3(NHC). *Organometallics* **2009**, *28* (22), 6458-6461. DOI: 10.1021/om900654g.
- (29) Vogiatzis, K. D.; Polynski, M. V.; Kirkland, J. K.; Townsend, J.; Hashemi, A.; Liu, C.; Pidko, E. A. Computational Approach to Molecular Catalysis by 3d Transition Metals: Challenges and Opportunities. *Chem. Rev.* **2019**, *119* (4), 2453-2523. DOI: 10.1021/acs.chemrev.8b00361.
- (30) Neese, F.; Wennmohs, F.; Becker, U.; Riplinger, C. The ORCA quantum chemistry program package. *The Journal of Chemical Physics* **2020**, *152* (22), 224108. DOI: 10.1063/5.0004608 (accessed 9/25/2023).
- (31) Neese, F. Software update: The ORCA program system—Version 5.0. *WIREs Computational Molecular Science* **2022**, *12* (5), e1606. DOI: https://doi.org/10.1002/wcms.1606 (accessed 2023/11/28).
- (32) Perdew, J. P. Density-functional approximation for the correlation energy of the inhomogeneous electron gas. *Physical Review B* **1986**, *33* (12), 8822-8824. DOI: 10.1103/PhysRevB.33.8822.

- (33) Grimme, S.; Antony, J.; Ehrlich, S.; Krieg, H. A consistent and accurate ab initio parametrization of density functional dispersion correction (DFT-D) for the 94 elements H-Pu. *The Journal of Chemical Physics* **2010**, *132* (15), 154104. DOI: 10.1063/1.3382344 (accessed 11/28/2023).
- (34) Grimme, S.; Ehrlich, S.; Goerigk, L. Effect of the damping function in dispersion corrected density functional theory. *Journal of Computational Chemistry* **2011**, *32* (7), 1456-1465. DOI: https://doi.org/10.1002/jcc.21759 (accessed 2023/11/28).
- (35) Eichkorn, K.; Treutler, O.; Öhm, H.; Häser, M.; Ahlrichs, R. Auxiliary basis sets to approximate Coulomb potentials (Chem. Phys. Letters 240 (1995) 283-290). *Chemical Physics Letters* **1995**, 242 (6), 652-660. DOI: https://doi.org/10.1016/0009-2614(95)00838-U.
- (36) Weigend, F.; Ahlrichs, R. Balanced basis sets of split valence, triple zeta valence and quadruple zeta valence quality for H to Rn: Design and assessment of accuracy. *Physical Chemistry Chemical Physics* **2005**, 7 (18), 3297-3305, 10.1039/B508541A. DOI: 10.1039/B508541A.
- (37) Hellweg, A.; Hättig, C.; Höfener, S.; Klopper, W. Optimized accurate auxiliary basis sets for RI-MP2 and RI-CC2 calculations for the atoms Rb to Rn. *Theoretical Chemistry Accounts* **2007**, *117* (4), 587-597. DOI: 10.1007/s00214-007-0250-5.
- (38) Anneser, M. R.; Powers, X. B.; Peck, K. M.; Jensen, I. M.; Jenkins, D. M. One Macrocyclic Ligand, Four Oxidation States: A 16-Atom Ringed Dianionic Tetra-NHC Macrocycle and Its Cr(II) through Cr(V) Complexes. *Organometallics* **2019**, *38* (17), 3369-3376. DOI: 10.1021/acs.organomet.9b00476.
- (39) Anneser, M. R.; Elpitiya, G. R.; Townsend, J.; Johnson, E. J.; Powers, X. B.; DeJesus, J. F.; Vogiatzis, K. D.; Jenkins, D. M. Unprecedented Five-Coordinate Iron(IV) Imides Generate Divergent Spin States Based on the Imide R-Groups. *Angewandte Chemie International Edition* **2019**, *58* (24), 8115-8118. DOI: https://doi.org/10.1002/anie.201903132 (accessed 2023/11/28). (40) Falivene, L.; Credendino, R.; Poater, A.; Petta, A.; Serra, L.; Oliva, R.; Scarano, V.; Cavallo, L. SambVca 2. A Web Tool for Analyzing Catalytic Pockets with Topographic Steric Maps. *Organometallics* **2016**, *35* (13), 2286-2293. DOI: 10.1021/acs.organomet.6b00371.
- (41) Lu, T.; Chen, F. Multiwfn: A multifunctional wavefunction analyzer. *Journal of Computational Chemistry* **2012**, *33* (5), 580-592. DOI: https://doi.org/10.1002/jcc.22885 (accessed 2023/11/29).
- (42) Cramer, S. A.; Hernández Sánchez, R.; Brakhage, D. F.; Jenkins, D. M. Probing the role of an FeIV tetrazene in catalytic aziridination. *Chemical Communications* **2014**, *50* (90), 13967-13970, 10.1039/C4CC05124F. DOI: 10.1039/C4CC05124F.
- (43) Mageed, A. H. Chemistry of macrocyclic tetracarbene complexes: Synthesis, structure, reactivity and catalytic application. *Journal of Organometallic Chemistry* **2019**, *902*, 120965. DOI: https://doi.org/10.1016/j.jorganchem.2019.120965.
- (44) Cramer, S. A.; Sturgill, F. L.; Chandrachud, P. P.; Jenkins, D. M. Overcoming NHCs neutrality: installing tetracarbenes on group 13 and 14 metals. *Dalton Transactions* **2014**, *43* (21), 7687-7690, 10.1039/C4DT00990H. DOI: 10.1039/C4DT00990H.
- (45) DeJesus, J. F.; Jenkins, D. M. A Chiral Macrocyclic Tetra-N-Heterocyclic Carbene Yields an "All Carbene" Iron Alkylidene Complex. *Chemistry A European Journal* **2020**, *26* (6), 1429-1435. DOI: https://doi.org/10.1002/chem.201905360 (accessed 2023/11/28).
- (46) Kück, J. W.; Anneser, M. R.; Hofmann, B.; Pöthig, A.; Cokoja, M.; Kühn, F. E. Fighting Fenton Chemistry: A Highly Active Iron(III) Tetracarbene Complex in Epoxidation Catalysis.

- *ChemSusChem* **2015**, *8* (23), 4056-4063. DOI: https://doi.org/10.1002/cssc.201500930 (accessed 2023/11/28).
- (47) Fei, F.; Lu, T.; Chen, X.-T.; Xue, Z.-L. Synthesis and structural characterization of metal complexes with macrocyclic tetracarbene ligands. *New Journal of Chemistry* **2017**, *41* (22), 13442-13453, 10.1039/C7NJ02485A. DOI: 10.1039/C7NJ02485A.
- (48) Jones, J. E.; Ruppel, J. V.; Gao, G.-Y.; Moore, T. M.; Zhang, X. P. Cobalt-Catalyzed Asymmetric Olefin Aziridination with Diphenylphosphoryl Azide. *The Journal of Organic Chemistry* **2008**, *73* (18), 7260-7265. DOI: 10.1021/jo801151x.
- (49) Tolman, C. A. Steric effects of phosphorus ligands in organometallic chemistry and homogeneous catalysis. *Chemical Reviews* **1977**, 77 (3), 313-348. DOI: 10.1021/cr60307a002.
- (50) Strohmeier, W.; Müller, F.-J. Klassifizierung phosphorhaltiger Liganden in Metallcarbonyl-Derivaten nach der π -Acceptorstärke. *Chemische Berichte* **1967**, *100* (9), 2812-2821. DOI: https://doi.org/10.1002/cber.19671000907 (accessed 2023/11/28).
- (51) Lundgren, R. J.; Stradiotto, M. Key Concepts in Ligand Design. In *Ligand Design in Metal Chemistry*, 2016; pp 1-14.
- (52) Riener, K.; Haslinger, S.; Raba, A.; Högerl, M. P.; Cokoja, M.; Herrmann, W. A.; Kühn, F. E. Chemistry of Iron N-Heterocyclic Carbene Complexes: Syntheses, Structures, Reactivities, and Catalytic Applications. *Chemical Reviews* **2014**, *114* (10), 5215-5272. DOI: 10.1021/cr4006439.
- (53) Kirkland, J. K.; Khan, S. N.; Casale, B.; Miliordos, E.; Vogiatzis, K. D. Ligand field effects on the ground and excited states of reactive FeO2+ species. *Physical Chemistry Chemical Physics* **2018**, *20* (45), 28786-28795, 10.1039/C8CP05372C. DOI: 10.1039/C8CP05372C.
- (54) Srnec, M.; Wong, S. D.; England, J.; Que, L.; Solomon, E. I. π -Frontier molecular orbitals in S = 2 ferryl species and elucidation of their contributions to reactivity. *Proceedings of the National Academy of Sciences* **2012**, *109* (36), 14326-14331. DOI: 10.1073/pnas.1212693109 (accessed 2023/11/28).
- (55) Wong, S. D.; Srnec, M.; Matthews, M. L.; Liu, L. V.; Kwak, Y.; Park, K.; Bell Iii, C. B.; Alp, E. E.; Zhao, J.; Yoda, Y.; et al. Elucidation of the Fe(iv)=O intermediate in the catalytic cycle of the halogenase SyrB2. *Nature* **2013**, *499* (7458), 320-323. DOI: 10.1038/nature12304.
- (56) Srnec, M.; Wong, S. D.; Matthews, M. L.; Krebs, C.; Bollinger, J. M., Jr.; Solomon, E. I. Electronic Structure of the Ferryl Intermediate in the α-Ketoglutarate Dependent Non-Heme Iron Halogenase SyrB2: Contributions to H Atom Abstraction Reactivity. *Journal of the American Chemical Society* **2016**, *138* (15), 5110-5122. DOI: 10.1021/jacs.6b01151.
- (57) Pandey, B.; Jaccob, M.; Rajaraman, G. Mechanistic insights into intramolecular ortho-amination/hydroxylation by nonheme FeIV \square NTs/FeIV \square O species: the σ vs. the π channels. *Chemical Communications* **2017**, *53* (22), 3193-3196, 10.1039/C6CC08761B. DOI: 10.1039/C6CC08761B.
- (58) Moreau, Y.; Chen, H.; Derat, E.; Hirao, H.; Bolm, C.; Shaik, S. NR Transfer Reactivity of Azo-Compound I of P450. How Does the Nitrogen Substituent Tune the Reactivity of the Species toward CH and CC Activation? *The Journal of Physical Chemistry B* **2007**, *111* (34), 10288-10299. DOI: 10.1021/jp0743065.
- (59) Kumar, S.; Faponle, A. S.; Barman, P.; Vardhaman, A. K.; Sastri, C. V.; Kumar, D.; de Visser, S. P. Long-Range Electron Transfer Triggers Mechanistic Differences between Iron(IV)-Oxo and Iron(IV)-Imido Oxidants. *Journal of the American Chemical Society* **2014**, *136* (49), 17102-17115. DOI: 10.1021/ja508403w.

(60) Mitoraj, M.; Michalak, A. Natural orbitals for chemical valence as descriptors of chemical bonding in transition metal complexes. *Journal of Molecular Modeling* **2007**, *13* (2), 347-355. DOI: 10.1007/s00894-006-0149-4.